

Article

Nitrogen-Rich Energetic Metal-Organic Framework: Synthesis, Structure, Properties, and Thermal Behaviors of Pb(II) Complex Based on *N,N*-Bis(1*H*-tetrazole-5-yl)-Amine

Qiangqiang Liu ^{1,2}, Bo Jin ^{2,*}, Qingchun Zhang ², Yu Shang ², Zhicheng Guo ³, Bisheng Tan ⁴ and Rufang Peng ^{1,2,*}

¹ Research Center of Laser Fusion, China Academy of Engineering Physics, Mianyang 621010, China; liuqq006@mail.ustc.edu.cn

² State Key Laboratory Cultivation Base for Nonmetal Composites and Functional Materials, Southwest University of Science and Technology, Mianyang 621010, China; zhangqingchun@live.cn (Q.Z.); 410621b03kq.cdb@sina.cn (Y.S.)

³ School of National Defence Science and Technology, Southwest University of Science and Technology, Mianyang 621010, China; zcguo@swust.edu.cn

⁴ Institute of Chemical Materials, Chinese Academy of Engineering Physics, Mianyang 621010, China; cqtbs@163.com

* Correspondence: jinbo0428@163.com (B.J.); rfpeng2006@163.com (R.P.); Tel.: +86-816-6088-257 (B.J. & R.P.)

Academic Editor: Umit B. Demirci

Received: 20 June 2016; Accepted: 25 July 2016; Published: 10 August 2016

Abstract: The focus of energetic materials is on searching for a high-energy, high-density, insensitive material. Previous investigations have shown that 3D energetic metal–organic frameworks (E-MOFs) have great potential and advantages in this field. A nitrogen-rich E-MOF, Pb(bta)·2H₂O [N% = 31.98%, H₂bta = *N,N*-Bis(1*H*-tetrazole-5-yl)-amine], was prepared through a one-step hydrothermal reaction in this study. Its crystal structure was determined through single-crystal X-ray diffraction, Fourier transform infrared spectroscopy, and elemental analysis. The complex has high heat denotation (16.142 kJ·cm^{−3}), high density (3.250 g·cm^{−3}), and good thermostability ($T_{dec} = 614.9$ K, 5 K·min^{−1}). The detonation pressure and velocity obtained through theoretical calculations were 43.47 GPa and 8.963 km·s^{−1}, respectively. The sensitivity test showed that the complex is an impact-insensitive material (IS > 40 J). The thermal decomposition process and kinetic parameters of the complex were also investigated through thermogravimetry and differential scanning calorimetry. Non-isothermal kinetic parameters were calculated through the methods of Kissinger and Ozawa-Doyle. Results highlighted the nitrogen-rich MOF as a potential energetic material.

Keywords: nitrogen-rich materials; energetic materials; energetic MOFs

1. Introduction

In the past decade, metal-organic frameworks (MOFs) have elicited much interest in chemistry, material science, medicine, and environmental science [1–9] because of their stable architectures, controllable structures, modifiable properties, and potential applications in gas storage [10–13], chemical separation [14–17], catalysis [18–21], chemical sensor technology [5], drug delivery [22–24], and so on. Many investigators have recently demonstrated the possibility of using nitrogen-rich MOFs as high explosives [25–48]. MOFs consist of metal ions (Pb²⁺, Ag⁺, etc.), energetic anions (e.g., N₃[−] and NO₃[−]), or simple energetic ligands (triazole, tetrazole, tetrazine, hydrazine, etc.). The network structures of energetic MOFs (E-MOFs) can be designed as 1D, 2D, or 3D architectures (Figure 1) depending on the metal ion geometry and binding mode of the bridging energetic ligands.

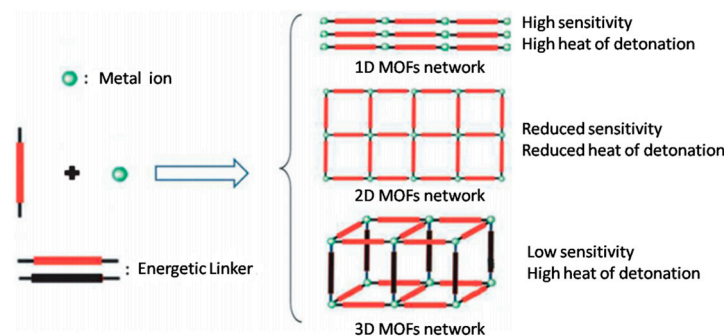


Figure 1. Design strategy for 1D, 2D, and 3D energetic MOFs (Reprinted from Refs. [28,49]. (Copyright 2013 and 2014 Wiley).

Several 1D E-MOFs (CHP: $\text{CoN}_{10}\text{H}_{20}\text{Cl}_2\text{O}_8$, $\text{N}\% = 33.49\%$, $\rho = 1.948 \text{ g}\cdot\text{cm}^{-3}$, NHP: $\text{NiN}_{10}\text{H}_{20}\text{O}_8\text{Cl}_2$, NHN: $\text{NiN}_8\text{H}_{12}\text{O}_6$; Figure 2) and 2D E-MOFs (CHHP: $\text{Co}_4\text{C}_4\text{H}_{48}\text{N}_{24}\text{O}_{26}\text{Cl}_4$, $\text{N}\% = 27.41\%$, $\rho = 2.0 \text{ g}\cdot\text{cm}^{-3}$; ZnHHP: $\text{Zn}_4\text{C}_4\text{H}_{40}\text{N}_{20}\text{O}_{26}\text{Cl}_4$, $\text{N}\% = 23.57\%$, $\rho = 2.117 \text{ g}\cdot\text{cm}^{-3}$) were developed by Hope-Weeks et al. through a combination of metal ion, energetic anion (ClO_4^- and NO_3^-), and non-bridged ligand (hydrazine) [25,27]. 1D E-MOFs have high detonation heat but are very sensitive. The sensitivity and detonation heat of 2D E-MOFs are lower than those of 1D E-MOFs. Different from 1D linear and 2D layered structures, 3D frameworks possess more complicated connection modes, which could further enhance structural reinforcement and thus improve the stability and energetic properties [29,49]. In 2013, two 3D E-MOFs, namely, $\text{CuC}_{12}\text{H}_{12}\text{N}_{26}\text{O}_6$ ($\text{N}\% = 53.35\%$, $\rho = 1.68 \text{ g}\cdot\text{cm}^{-3}$, $\text{IS} = 22.5 \text{ J}$) and $\text{AgC}_6\text{H}_6\text{N}_{13}\text{O}_3$ ($\text{N}\% = 53.35\%$, $\rho = 2.16 \text{ g}\cdot\text{cm}^{-3}$, $\text{IS} = 30 \text{ J}$), were introduced by Pang et al. for the first time [28]. The sensitivities of these 3D MOFs are significantly lower than those of reported energetic coordination polymers, such as 1D (CHP, $\text{IS} = 0.5 \text{ J}$) and 2D (ZnHHP, $\text{IS} = 2.5 \text{ J}$; CHHP, $\text{IS} = 0.8 \text{ J}$) MOFs. An increasing number of investigations on E-MOFs as new-generation high explosives were reported by Chen et al. [32,33,36,38–40,42,44,45,50,51], Pang et al. [28,48,52], Shreeve et al. [49,53], and so on [41,47,54–56] because of the advantages of 3D MOFs.

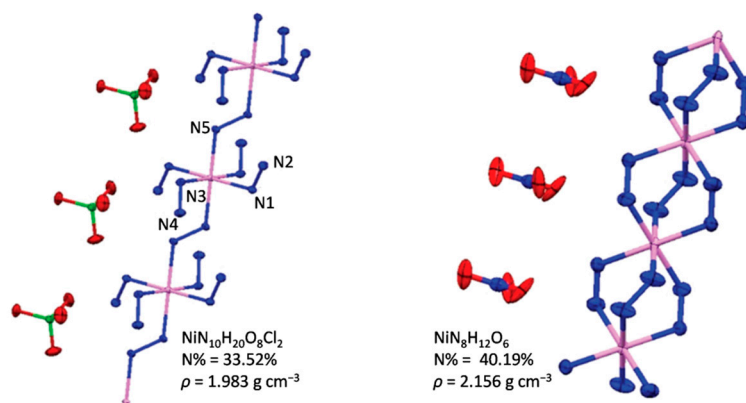


Figure 2. 1D energetic MOFs of nickel hydrazine-perchlorate (NHP, left) and nickel hydrazine-nitrate (NHN, right) (Reprinted from Ref. [25]. Copyright 2012 American Chemical Society).

N,N-Bis(1*H*-tetrazole-5-yl)-amine (H_2bta), a compound with high nitrogen content ($\text{N}\% = 82.34\%$), had its first single crystal structure and copper complexes reported by Klapötke et al. [57,58]. Shreeve et al. conducted extensive research on the energetic salts of H_2bta [59–61] and found that the salts exhibit excellent energetic properties. The investigations also showed that H_2bta may be an excellent energetic ligand to construct 3D MOFs for the following reasons [51]. First, the rigid structure

of H₂bta cannot only promote structural stability but can also improve the energetic performance of MOFs. Second, the versatile chelating-bridging coordination modes are propitious to the construction of high-dimensional 3D MOFs. Third, nitrogen atoms are involved in hydrogen-bond motifs to capture energetic moieties. Fourth, the predominant decomposition products are environmentally benign nitrogen gases. Fifth, the azide group hidden in aminotetrazole is the best stable moiety by virtue of the extended 6 π system. Therefore, many MOFs based on H₂bta, such as Cu(II) [39,62–64], Co(II,III) [36,50], Fe(III) [65], Mn(II) [66,67], Zn(II) [46,66,68,69], Cd(II) [66] MOFs, and others [70], have been obtained and investigated.

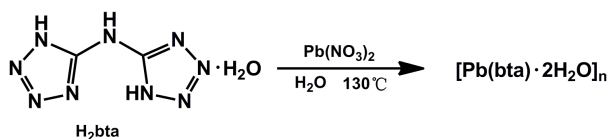
Pb(II)-bta MOFs (The Cambridge Crystallographic Data Centre (CCDC) numbers 650737, 721842, 721843) were synthesized originally via a two-step approach, and there were no reports about their energetic properties [71]. In this study, [Pb(bta)·2H₂O]_n (CCDC number 1478651) was synthesized via a one-step hydrothermal reaction without any other assistant ligands (such as 2,2-bipyridine, 1,10-phenanthroline). The single crystal X-ray experiment revealed the coordination mode of bta²⁻ with Pb²⁺. The energetic properties (detonation velocity, detonation pressure, and impact sensitivity) and thermal behavior of [Pb(bta)·2H₂O]_n were also investigated. The thermodynamic parameters were obtained based on the reaction thermodynamic and kinetic equations. As expected, the complex exhibited high thermostability, excellent detonation properties, and acceptable sensitivity to impact. These features suggest potential applications as an energetic material.

2. Results and Discussion

General caution: H₂bta and its derivatives are potentially explosive and should be handled in small quantities. Appropriate safety precautions should be taken, and larger scale synthesis is not recommended.

2.1. Synthesis of the Complex

H₂bta·H₂O was synthesized according to the literature [58]. Herein, three methods were used to synthesize Pb(II) coordination compounds based on H₂bta, but only one route obtained the target complex successfully. As shown in Scheme 1, a mixture of Pb(NO₃)₂ (0.1 mmol) and H₂bta·H₂O (0.13 mmol) in H₂O (4 mL) was sealed in a 10-mL Teflon-lined stainless autoclave and heated at 130 °C under autogenous pressure for three days and then cooled to room temperature over a further threedays. Colorless prismatic single-crystals suitable for X-ray diffraction were obtained.



Scheme 1. Synthesis of energetic 3D MOFs [Pb(bta)·2H₂O]_n.

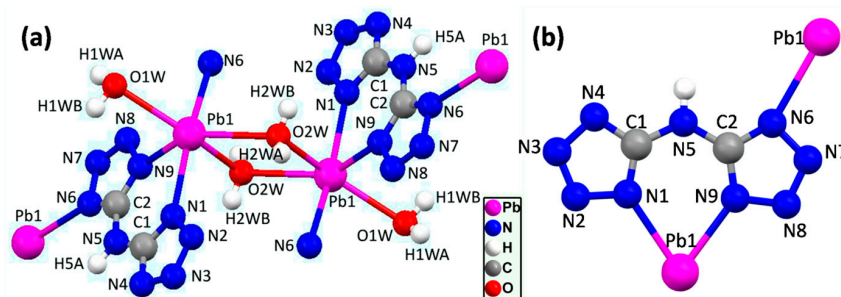
2.2. Crystal Structure of the Complex

The X-ray crystallographic and structural refinement data are summarized in Table 1, and the structures are shown in Figures 3–5. Further information on the crystal structure determination is provided in the Supplementary Materials (Tables S1–S6). Analysis of the X-ray crystallographic data for the complex shows that it crystallizes in the monoclinic space group $P2_1/n$ with a calculated density of 3.250 g·cm⁻³ based on four molecules packed in the unit-cell volume of 806.0(10) Å³. Density is a highly important physical property of energetic materials. Herein, because metal coordination can improve the densities of energetic materials, the density values of complex is much higher than that of the free ligand (1.693 g·cm⁻³).

Table 1. Crystal data and structure refinement data of [Pb(bta)-2H₂O]_n.

| Empirical Formula | C ₂ H ₅ N ₉ O ₂ Pb |
|---|--|
| Formula weight | 394.34 |
| Crystal Color | colorless |
| Crystal size (mm ³) | 0.21 × 0.20 × 0.19 mm |
| Crystal system | Monoclinic |
| Space group | <i>P</i> 2 ₁ / <i>n</i> |
| <i>a</i> (Å) | 6.592(5) |
| <i>b</i> (Å) | 11.987(9) |
| <i>c</i> (Å) | 10.552(8) |
| α (°) | 90 |
| β (°) | 104.856(12) |
| γ (°) | 90 |
| <i>V</i> (Å ³) | 806.0(10) |
| <i>Z</i> | 4 |
| ρ_{calcd} (g·cm ⁻³) | 3.250 |
| <i>T</i> (K) | 150(2) |
| <i>F</i> (000) | 712 |
| θ (°) | 2.62 to 25.00 |
| <i>R</i> _{int} | 0.0425 |
| Data | 1423 |
| Restraints | 4 |
| parameters | 127 |
| GOF ^a on <i>F</i> ² | 1.051 |
| <i>R</i> ₁ ^b (<i>I</i> > 2σ(<i>I</i>)) | 0.0241 |
| ωR_2 ^c (<i>I</i> > 2σ(<i>I</i>)) | 0.0655 |
| <i>R</i> ₁ (all data) | 0.0261 |

^a GOF = Goodness of Fit; ^b $R_1 = \sum ||F_o| - |F_c|| / \sum |F_o|$; ^c $\omega R_2 = [(\omega(F_o^2 - F_c^2)^2) / \omega(F_o^2)^2]^{1/2}$.

**Figure 3.** Ball-and-stick molecular structure of [Pb(bta)-2H₂O] (a) and coordination mode of ligand (b).

The asymmetric unit is crystallographically independent with one Pb(II) ion, one bta²⁻ ligand, and two coordination water molecules (Figure 3a). Figure 3a shows that each Pb(II) ion is coordinated by three nitrogen atoms from two bta²⁻ ligands and three oxygen atoms from water molecules. An irregular octahedral geometry is exhibited. Compared with the structure of H₂bta [58], all of the bond lengths and angles are slightly changed, which may be caused by the negative charge on the anion rings and the coordination environment. The C–N bond lengths of C1–N1 [1.322(9) Å], C1–N4 [1.322(9) Å], C1–N5 [1.379(9) Å], C2–N5 [1.377(8) Å], C2–N6 [1.330(8) Å], and C2–N9 [1.328(8) Å] are between the standard C–N single bond (1.47 Å) and standard C=N double bond (1.32 Å) lengths and are indicative of an aromatic system [72,73]. Meanwhile, the N–N bond lengths of N1–N2 [1.376(7) Å], N2–N3 [1.284(9) Å], N3–N4 [1.350(8) Å], N6–N7 [1.347(9) Å], N7–N8 [1.306(8) Å], and N8–N9 [1.369(8) Å] also fit between the standard N–N single bond (1.45 Å) and standard N=N double bond (1.25 Å) lengths [74,75], which further confirm the conjugated and aromatic system. In addition, the bond angles C2–N5–C1 [125.0(6)°], N4–C1–N5 [112.8(6)°], N5–C2–N9

[127.2(6)°], and N6–C2–N9 [111.9(6)°] are slightly larger than those of H₂bta because of the influence of the coordination environment. Figure 3b shows that the coordination mode of the ligand has three coordinated nitrogen atoms (N1, N9, and N6) in each bta²⁻. Atoms N1 and N9 in the ligand adopt chelating modes to connect to Pb(II) ion, whereas atom N6 adopts monodentate bridging modes to link with other Pb(II) ions.

The packing diagram of the complex viewed down the *a*-axis, *b*-axis, and the *a*–*c* diagonal is shown in Figure 4. The adjacent Pb(II) ions are bridged by two oxygen atoms from water in an antiparallel manner, with a Pb...Pb separation distance of 4.484 Å, Pb1–O1W distance of 2.670 Å, Pb1–O2W distance of 2.586 Å, O2W–Pb1–O2W angle of 69.01°, and O2W–Pb1–O1W angle of 144.05°. The view down the *b*-axis shows that a series of parallel rhombi are formed by the adjacent Pb1 and O2w. The torsion angles [i.e., N3–N2–N1–C1 (–0.2°), N9–Pb1–N1–N2 (179.2°), N1–N2–N3–N4 (–0.7°), and C2–N5–C1–N4 (179.3°)] are close to ±180° and 0°, which illustrates that Pb(II) and its chelating mode ligand are strictly coplanar. In addition, five types of hydrogen bonds [N5–H5A...N8^{3#} = 3.032 Å, O1W–H1WA...N2^{4#} = 2.841 Å, O1W–H1WB...N3^{5#} = 3.411 Å, O2W–H2WA...N3^{6#} = 2.856 Å, and O2W–H2WB...O1W^{7#} = 2.715 Å; symmetry transformations used to generate equivalent atoms: (^{3#} *x* – 1/2, –*y* + 3/2, *z* – 1/2), (^{4#} –*x* + 1/2, *y* – 1/2, –*z* + 3/2), (^{5#} –*x*, –*y* + 2, –*z* + 1), (^{6#} –*x* – 1/2, –*y* – 1/2, –*z* + 3/2), and (^{7#} *x* – 1, *y*, *z*)] (others are listed in the Supplementary Materials) exist in the target complex and further enhance the structural reinforcement. The complex [Pb(bta)·2H₂O]_n has a good symmetrical and ordered 3D energetic framework.

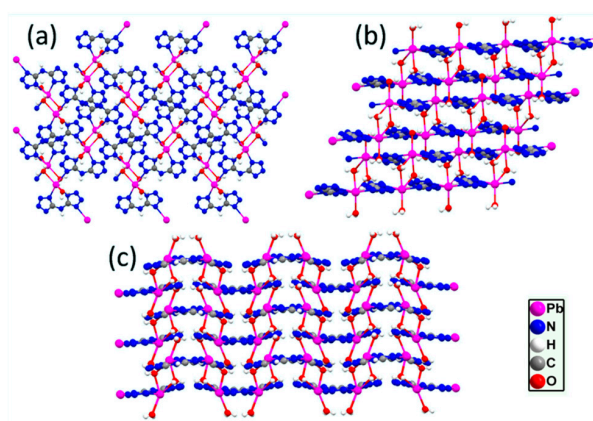


Figure 4. Ball-and-stick packing diagram of [Pb(bta)·2H₂O]_n viewed down the *a*-axis (a); *b*-axis (b); and *a*–*c* diagonal (c).

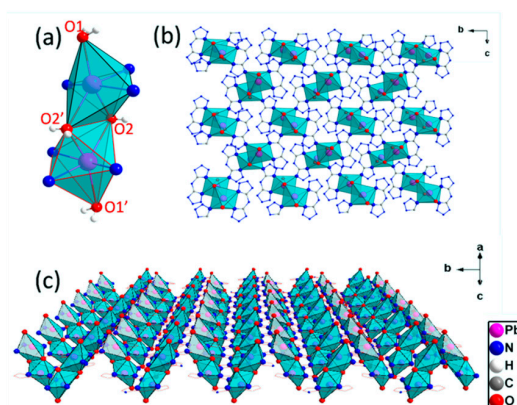


Figure 5. Coordination polyhedron geometry of [Pb(bta)·2H₂O]_n (a) polyhedrons with Pb(II) as the center viewed down *a*-axis (b) and the *a*–*c* diagonal (c).

The coordination polyhedron geometry of the complex is shown in Figure 5. $\text{Pb}(\text{bta})\cdot 2\text{H}_2\text{O}$ is a six-coordinate complex, and its polyhedron with $\text{Pb}(\text{II})$ as the center is an irregular octahedral geometry. The basal plane of the octahedron is formed by three nitrogen atoms and $\text{O}2'$ atoms, and the vertexes are occupied by $\text{O}1$ and $\text{O}2$ atoms (Figure 5a). Two adjacent octahedrons share the $\text{O}2\cdots\text{O}2'$ edge. Figure 5c shows that the planes that cross the $\text{Pb}(\text{II})$ ions in two interval polyhedrons are parallel. The two planes through the $\text{Pb}(\text{II})$ ions in two adjacent polyhedrons intersect, and the dihedral angle of the two planes is 33.8° .

2.3. Thermal Decomposition and Non-Isothermal Kinetics Analysis

2.3.1. Thermal Decomposition

Approximately 1.0 mg of the complex was tested through differential scanning calorimetry (DSC) in an open crucible at a heating rate of $5\text{ K}\cdot\text{min}^{-1}$ under nitrogen atmosphere to determine the melting points and decomposition temperatures. One endothermic process (loss of crystal water) peak and one exothermic process (decomposition) peak at 412.4 K and 614.9 K, respectively, are visible in the DSC curve (Figure 6). The relevant exothermic enthalpy change of the compound is $352.1\text{ kJ}\cdot\text{mol}^{-1}$. Therefore, this metal-organic crystal containing the bta^{2-} ligand possesses sufficient thermal stability to be an energetic material. In addition, the effect on T_p by the particle size were also investigated (Figures S2 and S3). The thermal behavior of millimeter sized single crystals and micron sized crystals were studied by DSC at the heating rate of $10\text{ K}\cdot\text{min}^{-1}$ under nitrogen atmosphere. The peak decomposition temperature of micron sized crystals MOF (about $10\text{ }\mu\text{m}$) is 615.4 K, which is lower than that of single crystals MOF ($T_p = 620.1\text{ K}$). The results are consistent with the reference by Cacho-Bailo et al. [76].

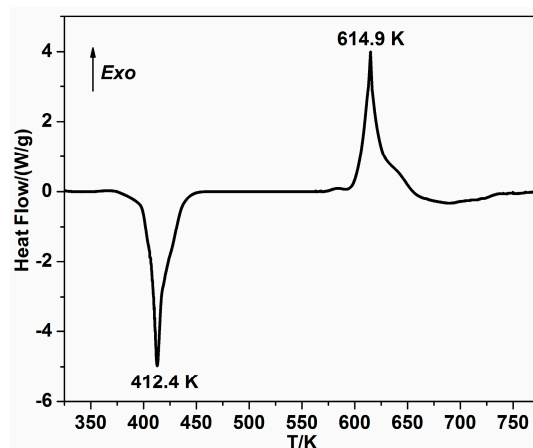


Figure 6. DSC curve of $[\text{Pb}(\text{bta})\cdot 2\text{H}_2\text{O}]_n$ at a heating rate of $5\text{ K}\cdot\text{min}^{-1}$.

The decomposition process of the complex was also investigated through the thermogravimetric analysis (TGA) at a heating rate of $5\text{ K}\cdot\text{min}^{-1}$ in nitrogen atmosphere. Figure 7 shows that the decomposition process of the complex can be divided into two steps, and the total mass loss is 48.09%. The first process in the range of 393 K–443 K was confirmed as the loss of crystal water (observed 9.24%, calculated 9.13%). This result indicates that the water molecules in the title complex were stable before 443 K. The second process from 581 to 657 K was considered the collapse of the structures related to the nitrogen-rich bta^{2-} groups.

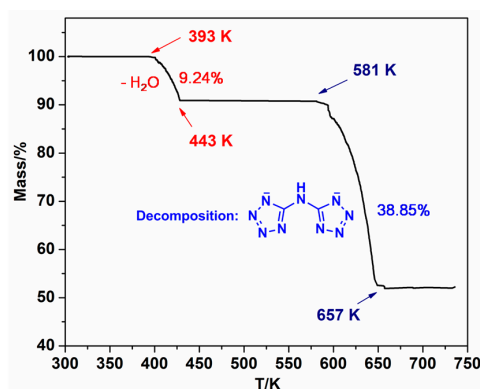


Figure 7. TGA curve of $[\text{Pb}(\text{bta})\cdot 2\text{H}_2\text{O}]_n$ at a heating rate of $5 \text{ K}\cdot\text{min}^{-1}$.

2.3.2. Non-Isothermal Kinetics Analysis

Kissinger's [77] and Ozawa's methods [78,79] were used to determine the kinetics parameters based on the exothermic peaks temperature measured from DSC curves with four different heating rates ($5, 10, 15, 20 \text{ K}\cdot\text{min}^{-1}$; Figure 8).

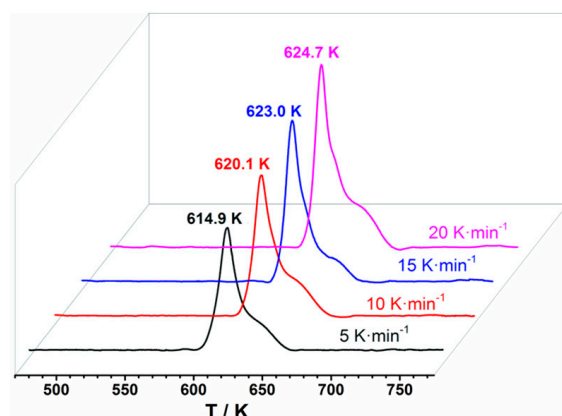


Figure 8. DSC curves of $[\text{Pb}(\text{bta})\cdot 2\text{H}_2\text{O}]_n$ at different heating rate.

Using the values of peak temperature, Kissinger Equation (Equation (1) in Section 3) and Ozawa-Doyle (Equation (2) in Section 3), the apparent activation energy (E) and pre-exponential factor (A) were calculated. The calculated results including linear correlation coefficient r are shown in Table 2. The results show that the value of E (about $430 \text{ kJ}\cdot\text{mol}^{-1}$) is higher than that of 1,3,5-trinitrohexahydro-1,3,5-triazine (RDX, about $142 \text{ kJ}\cdot\text{mol}^{-1}$) [62], cyclotetramethylene tetranitramine (HMX, about $238 \text{ kJ}\cdot\text{mol}^{-1}$) [62] and 2,4,6,8,10,12-hexanitro-2,4,6,8,10,12-hexaazatetracyclo [5.5.0.0.0] dodecane (CL-20, about $200 \text{ kJ}\cdot\text{mol}^{-1}$) [80,81], which is in accordance with its excellent thermostability.

Table 2. The calculated kinetic parameters for the exothermic decomposition processes of $[\text{Pb}(\text{bta})\cdot 2\text{H}_2\text{O}]_n$.

| $\beta/(\text{K}\cdot\text{min}^{-1})$ | $T_p/(\text{K})$ | Kissinger | | | Ozawa-Doyle | |
|--|------------------|-------------------------------------|---------|--------|-------------------------------------|--------|
| | | $E/(\text{kJ}\cdot\text{mol}^{-1})$ | $\ln A$ | r | $E/(\text{kJ}\cdot\text{mol}^{-1})$ | r |
| 5 | 614.9 | | | | | |
| 10 | 620.1 | 436.1 | 84.93 | 0.9984 | 424.6 | 0.9984 |
| 15 | 623.0 | | | | | |
| 20 | 624.7 | | | | | |

2.4. Energetic Properties

2.4.1. Heat Detonation of Complex

We selected an identical method for CHP and NHP to estimate the detonation heat (ΔH_{det}) of the compound and compare it with the values for E-MOFs and classical energetic materials [25]. For the complex, Pb, N₂, H₂O, NH₃, and C were assumed to be the final decomposition products of the organic part of the framework, and all non-metal-containing products, including water, were regarded as gas. The detonation reaction considered for the compound is described by Equation (3) (see Section 3), and the heat detonation value was obtained with Equation (4) (see Section 3), which was developed from known ΔH_{det} data for 11 commonly used high explosives.

Heat of detonation (ΔH_{det}) was calculated to be 4.966 kJ·g⁻¹. It is higher than those of MOFs ([Pb(Htztr)(O)]_n, 0.94 kJ·g⁻¹; CHHP, 3.14 kJ·g⁻¹; ZnHHP, 2.93 kJ·g⁻¹) but lower than those of RDX (5.799 kJ·g⁻¹) and HMX (5.523 kJ·g⁻¹) (see in Table 3). Figure 9 shows that despite the lack of advantage of the ΔH_{det} of the per gram complex, the ΔH_{det} of per cm³ (16.142 kJ·cm⁻³) is higher than that of traditional explosives and E-MOFs, except for ATRZ-1 (ATRZ: 4,4'-azo-1,2,4-triazole) because of its high density.

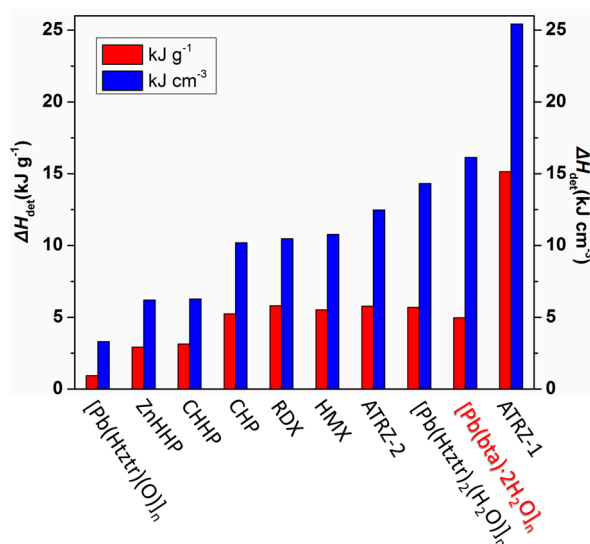


Figure 9. Bar chart representation of ΔH_{det} values in literature for common explosive materials and previously reported values for energetic MOFs along with the predicted ΔH_{det} value for [Pb(bta)₂·2H₂O]_n. The errorbars correspond to the 96% statistical-confidence level for these values.

2.4.2. Detonation Properties and Sensitivity

The performance of a high explosive is characterized by its detonation velocity, D (km·s⁻¹), and detonation pressure, P (GPa). The D and P of the complex were calculated with the Kamlet–Jacobs equations (see Equations (5)–(7) in Section 3), which are usually applied to E-MOFs reported previously. Table 3 shows a comparison of the physicochemical properties of several energetic materials and the complex. The D and P of the complex are 8.963 km·s⁻¹ and 47.47 GPa, respectively. Its D is higher than that of HMX (8.900 km·s⁻¹), RDX (8.600 km·s⁻¹), and other E-MOFs (6.205–8.226 km·s⁻¹), except for ATRZ-1 (9.160 km·s⁻¹).

Sensitivity deserves significant attention from researchers because it is closely linked with the safety of handling and applying explosives. The impact sensitivity (IS) of the compound was investigated for initial safety testing. Table 3 provides a summary of the data collected. The IS of [Pb(bta)₂·2H₂O]_n is more than 40 J, whereas the IS of RDX is 7.4 J under the same test condition. The IS of the complex is more insensitive than traditional explosives (HMX, 7.4 J; RDX, 7.4 J) and

reported energetic coordination polymers, such as 1D (CHP, IS = 0.5 J), 2D (ZnHHP, IS = 2.5 J; CHHP, IS = 0.8 J), and 3D (ATRZ-1, IS = 22.5 J) MOFs. These results reveal that the compound is insensitive to external stimuli because of the stabilized 3D covalent framework, in which the molecules are more rigid than those in 1D or 2D structures. Thus, $[\text{Pb}(\text{bta})\cdot 2\text{H}_2\text{O}]_n$ can be classified as an impact-insensitive energetic material.

Table 3. Physicochemical properties of $[\text{Pb}(\text{bta})\cdot 2\text{H}_2\text{O}]_n$.

| | T_d^a | ρ^b | N ^c | ΔH_{det}^d | D^e | P^f | IS ^g |
|---|---------|----------|----------------|---------------------------|-------|-------|-----------------|
| $[\text{Pb}(\text{bta})\cdot 2\text{H}_2\text{O}]_n$ | 342 | 3.250 | 31.98 | 4.97 | 8.963 | 47.47 | >40.0 |
| CHP ^h [25] | 194 | 1.948 | 14.71 | 5.23 | 8.225 | 31.73 | 0.5 |
| CHHP ^h [27] | 231 | 2.000 | 28.25 | 3.14 | 6.205 | 17.96 | 0.8 |
| ZnHHP ^h [27] | 293 | 2.117 | 23.61 | 2.93 | 7.016 | 23.58 | 2.5 |
| ATRZ-1 ^h [29] | 243 | 1.680 | 53.35 | 15.14 | 9.160 | 35.68 | 22.5 |
| ATRZ-2 ^h [29] | 257 | 2.160 | 43.76 | 5.78 | 7.773 | 29.70 | 30.0 |
| $[\text{Pb}(\text{Htztr})_2^h (\text{H}_2\text{O})]_n$ [32] | 340 | 2.519 | 39.40 | 5.69 | 7.715 | 31.57 | >40.0 |
| $[\text{Pb}(\text{Htztr})(\text{O})]_n^h$ [32] | 318 | 3.511 | 27.20 | 0.94 | 8.122 | 40.12 | >40.0 |
| HMX [25] | 287 | 1.950 | 37.84 | 5.52 | 8.900 | 38.39 | 7.4 |
| RDX [25] | 210 | 1.806 | 37.80 | 5.80 | 8.600 | 33.92 | 7.4 |

^a Decomposition temperature; ^b Density from X-ray diffraction analysis ($\text{g}\cdot\text{cm}^{-3}$); ^c Nitrogen content (%);

^d The heat of detonation ($\text{kJ}\cdot\text{g}^{-1}$); ^e Detonation velocity ($\text{km}\cdot\text{s}^{-1}$); ^f Detonation pressure (GPa);

^g Impact sensitivity; ^h CHP = cobalt hydrazine perchlorate; CHHP = cobalt hydrazine hydrazinecarboxylate perchlorate; ZnHHP = zinc hydrazine hydrazinecarboxylate perchlorate; ATRZ = 4,4'-azo-1,2,4-triazole; Htztr = 3-(tetrazol-5-yl)triazole.

3. Materials and Methods

The FT-IR spectrum was recorded on Nicolet 380 FT-IR spectrophotometer (Thermo Fisher Nicolet, Waltham, MI, USA) employing a KBr matrix with a resolution of 4 cm^{-1} , in the wavelength range of 400 cm^{-1} to 4000 cm^{-1} . Elemental analysis was performed on a Vario ELCUBE Elemental Analyzer (Elementar, Hanau, Germany). DSC was performed by a Q200 DSC instrument (TA Instruments, New Castle, DE, USA) at a heating rate of 5, 10, 15 and $20\text{ K}\cdot\text{min}^{-1}$, respectively, in flowing high-purity nitrogen. Approx. 1.0 mg sample was sealed in aluminum pans in the temperature range of 313 to 773 K for DSC experiments. The sensitivity to impact stimuli was determined by fall hammer apparatus according to the standard staircase method (GJB of China). With a step of 0.04 cm, 50 ± 1 mg of test specimens were used and a 10-kg drop weight was allowed to fall freely from different heights. The results were reported in terms of height for 50% probability of explosion ($h_{50\%}$). The picture of micron sized crystal MOF was obtained by a microscope ($\times 1000$). Molecular structure packing diagram and coordination polyhedron geometry of $[\text{Pb}(\text{bta})\cdot 2\text{H}_2\text{O}]_n$ were drawn by Mercury and Diamond software (Diamond 3.1, Crystal Impact GbR, Bonn, Germany).

3.1. Synthesis of $[\text{Pb}(\text{bta})\cdot 2\text{H}_2\text{O}]_n$

Method 1: a mixture of $\text{Pb}(\text{NO}_3)_2$ (33 mg, 0.1 mmol) and $\text{H}_2\text{bta}\cdot\text{H}_2\text{O}$ (22 mg, 0.13 mmol) in H_2O (4 mL) was sealed in a 10-mL Teflon-lined stainless autoclave and heated at $200\text{ }^\circ\text{C}$ under autogenous pressure for 3 days and then cooled to room temperature over a further 3 days. Two colorless single-crystals (needle and prismatic crystals) were picked up and a single crystal test indicated they are two different crystals of $\text{Pb}(\text{N}_3)_2$. See the structures in Supplementary Materials (Figure S1, Tables S8–S12).

Method 2: a suspension of H_2O (8 mL) and Pb(II) complex (30 mg), which was obtained from Na_2bta and $\text{Pb}(\text{NO}_3)_2$ as raw materials by means of metathesis reaction, was sealed in a 10 mL Teflon-lined stainless autoclave. Both experiments were heated at $130\text{ }^\circ\text{C}$ and $200\text{ }^\circ\text{C}$, respectively, under autogenous pressure for 3 days and then cooled to room temperature over a further 3 days. Unfortunately, there were powder instead of crystals in Teflon autoclave.

Method 3: a mixture of $\text{Pb}(\text{NO}_3)_2$ (33 mg, 0.1 mmol) and $\text{H}_2\text{bta}\cdot\text{H}_2\text{O}$ (22 mg, 0.13 mmol) in H_2O (4 mL) was sealed in a 10-mL Teflon-lined stainless autoclave and heated at 130°C under autogenous pressure for 3 days and then cooled to room temperature over a further 3 days. Colorless prismatic single-crystals were picked up and yield 23.8 mg (61% based on Pb). DSC ($5\text{ K}\cdot\text{min}^{-1}$): 614.9 K(dec.). FT-IR (KBr) $\tilde{\nu}$: 3432(vs), 3292(s), 2921(m), 2854(m), 1623(vs), 1525(m), 1500(m), 1420(m), 1314(m), 1230(w), 1127(w), 1115(w), 1069(w), 1015(w), 794(m), 740(m). Elemental analysis ($\text{C}_2\text{H}_5\text{N}_9\text{O}_2\text{Pb}$, 394.34) Calcd: C 6.09%, H 1.28%, N 31.98%; Found: C 6.11%, H 1.30%, N 31.89%.

3.2. Single-Crystal X-ray Diffraction Analyses

The single-crystal X-ray experiments were performed on a Smart Apex CCD diffractometer (Bruker) (Bruker, Karlsruhe, Germany) equipped with graphite monochromatized $\text{Mo K}\alpha$ radiation ($\lambda = 0.71073\text{ \AA}$) using the ω and φ scan mode. The structure was solved by direct methods using SHELXS-97 (Göttingen, Germany) [82] and refined by means of full-matrix least-squares procedures on F^2 with the SHELXL-97 program [83]. All non-H atoms were located using subsequent Fourier-difference methods and refined anisotropically. In all cases, hydrogen atoms were placed in their calculated positions and thereafter allowed to ride on their parent atoms.

3.3. Equations for Calculating Non-Isothermal Kinetics

The Kissinger (1) and Ozawa-Doyle (2) Equations are as follows:

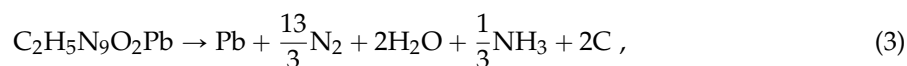
$$\ln[\beta/T_p^2] = \ln[AR/E_a] - [E_a/RT_p], \quad (1)$$

$$\lg\beta = C - 0.4567E_a/RT, \quad (2)$$

where β is the heating rate; T_p is the peak temperature; A is the pre-exponential factor; E is the apparent activation energy; and R is the gas constant ($8.314\text{ J}\cdot\text{K}^{-1}\cdot\text{mol}^{-1}$). Linear relationship of $\ln(\beta/T_p^2)$ and $\lg(\beta)$ vs. $1/T_p$ are shown in Supplementary Materials (Figure S4).

3.4. Calculation for Heat of Detonation

The complete detonation reactions are described by Equation (3). According to Ref. [25], Density Functional Theory (DFT) was used to calculate the energy of detonation (ΔE_{det}), from which ΔH_{det} was estimated by using a linear correlation Equation (4), and the calculated parameters was listed in Table S7. The DFT calculation for $[\text{Pb}(\text{bta})\cdot 2\text{H}_2\text{O}]_n$ was performed with the code DMOI3 [84] under 3D periodic boundary conditions employing the Monkhorst–Pack multiple K -point sampling of the Brillouin zone [85] and the Perdew–Becke–Ezerhoff (PBE) exchange–correlation function [86]:



$$\Delta H_{\text{det}} = 1.127 \Delta E_{\text{det}} + 0.046. \quad (4)$$

3.5. Calculation for Detonation Velocity and Detonation Pressure

The D and P of the complex were calculated by Kamlet–Jacobs Equations [28] as follows, which were usually applied to the E-MOFs reported previously:

$$D = 1.01\Phi^{1/2}(1 + 1.30\rho), \quad (5)$$

$$P = 1.558\Phi\rho^2, \quad (6)$$

$$\Phi = 31.68N(MQ)^{1/2} \quad (7)$$

where D is detonation velocity ($\text{km}\cdot\text{s}^{-1}$); P is detonation pressure (GPa); N is moles of detonation gases per gram of explosive; M is average molecular weight of the gases; Q is heat of detonation ($\text{kcal}\cdot\text{g}^{-1}$); ρ is density of explosive ($\text{g}\cdot\text{cm}^{-3}$); and Φ is a parameter determined by N , M and Q .

4. Conclusions

We successfully synthesized a nitrogen-rich E-MOF, namely, $\text{Pb}(\text{bta})\cdot 2\text{H}_2\text{O}$ [$\text{N}\% = 31.98\%$, $\text{H}_2\text{bta} = N,N\text{-Bis}(1H\text{-tetrazole-5-yl})\text{-amine}$]. It was characterized through various techniques, such as elemental analyses, Fourier transform infrared spectroscopy, TG, DSC, and single crystal X-ray diffraction. X-ray single crystal structure analysis showed that the crystal of the complex in the monoclinic space group $P2_1/n$ has a calculated density of $3.250\text{ g}\cdot\text{cm}^{-3}$. The DSC curve indicated that it has good thermostability. One endothermic process (around 412.4 K) and one exothermic process (around 614.9 K) exist at the heating rate $5\text{ K}\cdot\text{min}^{-1}$. The calculated results showed that the detonation heat, detonation pressure, and velocity are $4.966\text{ kJ}\cdot\text{g}^{-1}$ ($16.142\text{ kJ}\cdot\text{cm}^{-3}$), 43.47 GPa, and $8.963\text{ km}\cdot\text{s}^{-1}$, respectively. The sensitivity test showed that the complex is an impact-insensitive material ($\text{IS} > 40\text{ J}$). The thermal decomposition process and kinetic parameters of the complex were also investigated through TG and DSC. The non-isothermal kinetic parameters were calculated with the methods of Kissinger and Ozawa-Doyle. The activation energy value (about $430\text{ kJ}\cdot\text{mol}^{-1}$) is higher than that of RDX, HMX, and CL-20. Excellent impact sensitivity and high thermal stability depend on good detonation properties. The 3D MOF in this study has potential applications as an energetic material.

Supplementary Materials: The following are available online at www.mdpi.com/1996-1944/9/8/681/s1. Figure S1: Ball-and-stick molecular structure and packing diagram of $\text{Pb}(\text{N}_3)_2$, Figure S2: The pictures of single crystal MOF and micron sized crystal MOF, Figure S3: DSC curves of single crystal MOF and micron sized crystal MOF at the heating rate of $10\text{ K}\cdot\text{min}^{-1}$, Figure S4: Linear relationship of $\ln(\beta/T_p^2)$ and $\lg(\beta)$ vs. $1/T_p$, Table S1: Atomic coordinates and equivalent isotropic displacement parameters for $[\text{Pb}(\text{bta})\cdot 2\text{H}_2\text{O}]_n$, Table S2: Bond lengths and angles for $[\text{Pb}(\text{bta})\cdot 2\text{H}_2\text{O}]_n$, Table S3: Anisotropic displacement parameters for $[\text{Pb}(\text{bta})\cdot 2\text{H}_2\text{O}]_n$, Table S4: Hydrogen coordinates and isotropic displacement parameters for $[\text{Pb}(\text{bta})\cdot 2\text{H}_2\text{O}]_n$, Table S5: Torsion angles for $[\text{Pb}(\text{bta})\cdot 2\text{H}_2\text{O}]_n$, Table S6: Hydrogen bonds for $[\text{Pb}(\text{bta})\cdot 2\text{H}_2\text{O}]_n$, Table S7: Calculated parameters used in the detonation reactions, Table S8: Crystal data and structure refinement for $\text{Pb}(\text{N}_3)_2$, Table S9: Atomic coordinates and equivalent isotropic displacement parameters for $\text{Pb}(\text{N}_3)_2$, Table S10: Bond lengths and angles for $\text{Pb}(\text{N}_3)_2$, Table S11: Anisotropic displacement parameters for $\text{Pb}(\text{N}_3)_2$, Table S12: Torsion angles for $\text{Pb}(\text{N}_3)_2$.

Acknowledgments: We are grateful for financial support from the National Natural Science Foundation of China (project No. 51372211), the Open Project of State Key Laboratory Cultivation Base for Nonmetal Composites and Functional Materials (project No. 14zdfk05), Southwest University of Science and Technology Outstanding Youth Fundation (project No. 13zx9107), and the Institute of Chemical Materials, China Academy of Engineering Physics.

Author Contributions: Qiangqiang Liu and Bo Jin conceived and designed the experiments; Qiangqiang Liu and Yu Shang performed the experiments; Qiangqiang Liu, Qingchun Zhang, Yu Shang, Bo Jin and Rufang Peng analyzed the data; Zhicheng Guo and Bisheng Tan calculated the Denotation Heat of the complex and analyzed those data. Bo Jin and Rufang Peng directed the project and contributed reagents/materials/analysis tools; Qiangqiang Liu and Bo Jin wrote the paper.

Conflicts of Interest: The authors declare no conflict of interest.

References

1. Eddaoudi, M.; Moler, D.B.; Li, H.; Chen, B.; Reineke, T.M.; O'keeffe, M.; Yaghi, O.M. Modular chemistry: Secondary building units as a basis for the design of highly porous and robust metal-organic carboxylate frameworks. *Acc. Chem. Res.* **2001**, *34*, 319–330. [[CrossRef](#)] [[PubMed](#)]
2. Phan, A.; Doonan, C.J.; Uribe-Romo, F.J.; Knobler, C.B.; O'keeffe, M.; Yaghi, O.M. Synthesis, structure, and carbon dioxide capture properties of zeoliticimidazolate frameworks. *Acc. Chem. Res.* **2010**, *43*, 58–67. [[CrossRef](#)] [[PubMed](#)]
3. Das, M.C.; Xiang, S.; Zhang, Z.; Chen, B. Funktionelle gemischtmetall-organische gerüste mit metalloliganden. *Angew. Chem. Int. Ed.* **2011**, *123*, 10696–10707. [[CrossRef](#)]

4. Chang, B.K.; Bristowe, N.C.; Bristowe, P.D.; Cheetham, A.K. Van der waals forces in the perfluorinated metal-organic framework zinc 1,2-bis(4-pyridyl)ethane tetrafluoroterephthalate. *Phys. Chem. Chem. Phys.* **2012**, *14*, 7059–7064. [[CrossRef](#)] [[PubMed](#)]
5. Kreno, L.E.; Leong, K.; Farha, O.K.; Allendorf, M.; Van Deyne, R.P.; Hupp, J.T. Metal-organic framework materials as chemical sensors. *Chem. Rev.* **2012**, *112*, 1105–1125. [[CrossRef](#)] [[PubMed](#)]
6. Li, J.R.; Sculley, J.; Zhou, H.C. Metal-organic frameworks for separations. *Chem. Rev.* **2012**, *112*, 869–932. [[CrossRef](#)] [[PubMed](#)]
7. Liu, C.S.; Pilania, G.; Wang, C.; Ramprasad, R. How critical are the van der Waals interactions in polymer crystals? *J. Phys. Chem. A* **2012**, *116*, 9347–9352. [[CrossRef](#)] [[PubMed](#)]
8. Xuan, W.; Zhu, C.; Liu, Y.; Cui, Y. Mesoporous metal-organic framework materials. *Chem. Soc. Rev.* **2012**, *41*, 1677–1695. [[CrossRef](#)] [[PubMed](#)]
9. Furukawa, H.; Cordova, K.E.; O’Keeffe, M.; Yaghi, O.M. The chemistry and applications of metal-organic frameworks. *Science* **2013**, *341*, 1230444. [[CrossRef](#)] [[PubMed](#)]
10. Rosi, N.L.; Eckert, J.; Eddaoudi, M.; Vodak, D.T.; Kim, J.; O’Keeffe, M.; Yaghi, O.M. Hydrogen storage in microporous metal-organic frameworks. *Science* **2003**, *300*, 1127–1129. [[CrossRef](#)] [[PubMed](#)]
11. Belof, J.L.; Stern, A.C.; Eddaoudi, M.; Space, B. On the mechanism of hydrogen storage in a metal-organic framework material. *J. Am. Chem. Soc.* **2007**, *129*, 15202–15210. [[CrossRef](#)] [[PubMed](#)]
12. Bae, Y.S.; Snurr, R.Q. Development and evaluation of porous materials for carbon dioxide separation and capture. *Angew. Chem. Int. Ed.* **2011**, *50*, 11586–11596. [[CrossRef](#)] [[PubMed](#)]
13. Suh, M.P.; Park, H.J.; Prasad, T.K.; Lim, D.W. Hydrogen storage in metal-organic frameworks. *Chem. Rev.* **2012**, *112*, 782–835. [[CrossRef](#)] [[PubMed](#)]
14. Chen, B.; Liang, C.; Yang, J.; Contreras, D.S.; Clancy, Y.L.; Lobkovsky, E.B.; Yaghi, O.M.; Dai, S. A microporous metal-organic framework for gas-chromatographic separation of alkanes. *Angew. Chem. Int. Ed.* **2006**, *45*, 1390–1393. [[CrossRef](#)] [[PubMed](#)]
15. Bae, Y.S.; Mulfort, K.L.; Frost, H.; Ryan, P.; Punnathanam, S.; Broadbelt, L.J.; Hupp, J.T.; Snurr, R.Q. Separation of CO₂ from CH₄ using mixed-ligand metal-organic frameworks. *Langmuir* **2008**, *24*, 8592–8598. [[CrossRef](#)] [[PubMed](#)]
16. Bloch, E.D.; Queen, W.L.; Krishna, R.; Zadrozny, J.M.; Brown, C.M.; Long, J.R. Hydrocarbon separations in a metal-organic framework with open iron(II) coordination sites. *Science* **2012**, *335*, 1606–1610. [[CrossRef](#)] [[PubMed](#)]
17. Bloch, W.M.; Babarao, R.; Hill, M.R.; Doonan, C.J.; Sumbly, C.J. Post-synthetic structural processing in a metal-organic framework material as a mechanism for exceptional CO₂/N₂ selectivity. *J. Am. Chem. Soc.* **2013**, *135*, 10441–10448. [[CrossRef](#)] [[PubMed](#)]
18. Yoon, M.; Srirambalaji, R.; Kim, K. Homochiral metal-organic frameworks for asymmetric heterogeneous catalysis. *Chem. Rev.* **2012**, *112*, 1196–1231. [[CrossRef](#)] [[PubMed](#)]
19. Genna, D.T.; Wong-Foy, A.G.; Matzger, A.J.; Sanford, M.S. Heterogenization of homogeneous catalysts in metal-organic frameworks via cation exchange. *J. Am. Chem. Soc.* **2013**, *135*, 10586–10589. [[CrossRef](#)] [[PubMed](#)]
20. Nepal, B.; Das, S. Sustained water oxidation by a catalyst cage-isolated in a metal-organic framework. *Angew. Chem. Int. Ed.* **2013**, *52*, 7224–7227. [[CrossRef](#)] [[PubMed](#)]
21. Zhu, Q.L.; Li, J.; Xu, Q. Immobilizing metal nanoparticles to metal-organic frameworks with size and location control for optimizing catalytic performance. *J. Am. Chem. Soc.* **2013**, *135*, 10210–10213. [[CrossRef](#)] [[PubMed](#)]
22. Horcajada, P.; Serre, C.; Maurin, G.; Ramsahye, N.A.; Balas, F.; Vallet-Regí, M.; Sebban, M.; Taulelle, F.; Férey, G. Flexible porous metal-organic frameworks for a controlled drug delivery. *J. Am. Chem. Soc.* **2008**, *130*, 6774–6780. [[CrossRef](#)] [[PubMed](#)]
23. Horcajada, P.; Chalati, T.; Serre, C.; Gillet, B.; Sebrie, C.; Baati, T.; Eubank, J.F.; Heurtaux, D.; Clayette, P.; Kreuz, C.; et al. Porous metal-organic-framework nanoscale carriers as a potential platform for drug delivery and imaging. *Nat. Mater.* **2010**, *9*, 172–178. [[CrossRef](#)] [[PubMed](#)]
24. Della Rocca, J.; Liu, D.; Lin, W. Nanoscale metal-organic frameworks for biomedical imaging and drug delivery. *Acc. Chem. Res.* **2011**, *40*, 957–968. [[CrossRef](#)] [[PubMed](#)]
25. Bushuyev, O.S.; Brown, P.; Maiti, A.; Gee, R.H.; Peterson, G.R.; Weeks, B.L.; Hope-Weeks, L.J. Ionic polymers as a new structural motif for high-energy-density materials. *J. Am. Chem. Soc.* **2012**, *134*, 1422–1425. [[CrossRef](#)] [[PubMed](#)]

26. Tao, G.H.; Parrish, D.A.; Shreeve, J.M. Nitrogen-rich 5-(1-methylhydrazinyl)tetrazole and its copper and silver complexes. *Inorg. Chem.* **2012**, *51*, 5305–5312. [[CrossRef](#)] [[PubMed](#)]
27. Bushuyev, O.S.; Peterson, G.R.; Brown, P.; Maiti, A.; Gee, R.H.; Weeks, B.L.; Hope-Weeks, L.J. Metal-organic frameworks (MOFs) as safer, structurally reinforced energetics. *Chem. Eur. J.* **2013**, *19*, 1706–1711. [[CrossRef](#)] [[PubMed](#)]
28. Li, S.; Wang, Y.; Qi, C.; Zhao, X.; Zhang, J.; Zhang, S.; Pang, S. 3D energetic metal-organic frameworks: Synthesis and properties of high energy materials. *Angew. Chem. Int. Ed.* **2013**, *52*, 14031–14035. [[CrossRef](#)] [[PubMed](#)]
29. Wang, S.H.; Zheng, F.K.; Wu, M.F.; Liu, Z.F.; Chen, J.; Guo, G.C.; Wu, A.Q. Hydrothermal syntheses, crystal structures and physical properties of a new family of energetic coordination polymers with nitrogen-rich ligand *N*-[2-(1*H*-tetrazol-5-yl)ethyl]glycine. *CrystEngComm* **2013**, *15*, 2616–2623. [[CrossRef](#)]
30. Wu, B.D.; Zhang, T.L.; Li, Y.L.; Tong, W.C.; Zhou, Z.N.; Zhang, J.G.; Yang, L. Energetic Compounds Based on 4-Amino-1,2,4-triazole (ATZ) and Picrate (PA): $[\text{Zn}(\text{H}_2\text{O})_6](\text{PA})_2 \cdot 3\text{H}_2\text{O}$ and $[\text{Zn}(\text{ATZ})_3](\text{PA})_2 \cdot 2.5\text{H}_2\text{O}$. *Z. Anorg. Allg. Chem.* **2013**, *639*, 2209–2215. [[CrossRef](#)]
31. Wu, B.D.; Zhou, Z.N.; Li, F.G.; Yang, L.; Zhang, T.L.; Zhang, J.G. Preparation, crystal structures, thermal decompositions and explosive properties of two new high-nitrogen azide ethylenediamine energetic compounds. *New J. Chem.* **2013**, *37*, 646–653. [[CrossRef](#)]
32. Gao, W.; Liu, X.; Su, Z.; Zhang, S.; Yang, Q.; Wei, Q.; Chen, S.; Xie, G.; Yang, X.; Gao, S. High-energy-density materials with remarkable thermostability and insensitivity: Syntheses, structures and physicochemical properties of Pb(II) compounds with 3-(tetrazol-5-yl) triazole. *J. Mater. Chem. A* **2014**, *2*, 11958–11965. [[CrossRef](#)]
33. Liu, X.; Yang, Q.; Su, Z.; Chen, S.; Xie, G.; Wei, Q.; Gao, S. 3D high-energy-density and low sensitivity materials: Synthesis, structure and physicochemical properties of an azide–Cu(II) complex with 3,5-dinitrobenzoic acid. *RSC Adv.* **2014**, *4*, 16087–16093. [[CrossRef](#)]
34. Tong, W.C.; Yang, L.; Wu, B.D.; Zhang, T.L. Preparation, crystal structure, and thermal decomposition of a novel nitrogen-rich compound $\text{Zn}_3(\text{ATZ})_6(\text{N}_3)_6$ (ATZ = 4-amino-1,2,4-triazole, N% = 61.7%). *Z. Anorg. Allg. Chem.* **2014**, *640*, 980–985. [[CrossRef](#)]
35. Wu, B.D.; Bi, Y.G.; Li, F.G.; Yang, L.; Zhou, Z.N.; Zhang, J.G.; Zhang, T.L. A novel stable high-nitrogen energetic compound: Copper(II) 1,2-diaminopropane azide. *Z. Anorg. Allg. Chem.* **2014**, *640*, 224–228. [[CrossRef](#)]
36. Zhang, S.; Liu, X.; Yang, Q.; Su, Z.; Gao, W.; Wei, Q.; Xie, G.; Chen, S.; Gao, S. A new strategy for storage and transportation of sensitive high-energy materials: Guest-dependent energy and sensitivity of 3D metal-organic-framework-based energetic compounds. *Chem. Eur. J.* **2014**, *20*, 7906–7910. [[CrossRef](#)] [[PubMed](#)]
37. Chen, D.; Huang, S.; Zhang, Q.; Yu, Q.; Zhou, X.; Li, H.; Li, J. Two nitrogen-rich Ni(II) coordination compounds based on 5,5'-azotetrazole: Synthesis, characterization and effect on thermal decomposition for RDX, HMX and AP. *RSC Adv.* **2015**, *5*, 32872–32879. [[CrossRef](#)]
38. Feng, Y.; Liu, X.; Duan, L.; Yang, Q.; Wei, Q.; Xie, G.; Chen, S.; Yang, X.; Gao, S. In situ synthesized 3D heterometallic metal-organic framework (MOF) as a high-energy-density material shows high heat of detonation, good thermostability and insensitivity. *Dalton Trans.* **2015**, *44*, 2333–2339. [[CrossRef](#)] [[PubMed](#)]
39. Liu, X.; Gao, W.; Sun, P.; Su, Z.; Chen, S.; Wei, Q.; Xie, G.; Gao, S. Environmentally friendly high-energy MOFs: Crystal structures, thermostability, insensitivity and remarkable detonation performances. *Green Chem.* **2015**, *17*, 831–836. [[CrossRef](#)]
40. Liu, X.; Qu, X.; Zhang, S.; Ke, H.; Yang, Q.; Shi, Q.; Wei, Q.; Xie, G.; Chen, S. High-performance energetic characteristics and magnetic properties of a three-dimensional cobalt(II) metal-organic framework assembled with azido and triazole. *Inorg. Chem.* **2015**, *54*, 11520–11525. [[CrossRef](#)] [[PubMed](#)]
41. McDonald, K.A.; Seth, S.; Matzger, A.J. Coordination polymers with high energy density: An emerging class of explosives. *Cryst. Growth Des.* **2015**, *15*, 5963–5972. [[CrossRef](#)]
42. Qu, X.; Zhang, S.; Yang, Q.; Su, Z.; Wei, Q.; Xie, G.; Chen, S. Silver(I)-based energetic coordination polymers: Synthesis, structure and energy performance. *New J. Chem.* **2015**, *39*, 7849–7857. [[CrossRef](#)]
43. Xu, C.X.; Zhang, J.G.; Yin, X.; Jin, X.; Li, T.; Zhang, T.L.; Zhou, Z.N. Cd(II) complexes with different nuclearity and dimensionality based on 3-hydrazino-4-amino-1,2,4-triazole. *J. Solid State Chem.* **2015**, *226*, 59–65. [[CrossRef](#)]

44. Qu, X.N.; Zhang, S.; Wang, B.Z.; Yang, Q.; Han, J.; Wei, Q.; Xie, G.; Chen, S.P. An Ag(I) energetic metal-organic framework assembled with the energetic combination of furazan and tetrazole: Synthesis, structure and energetic performance. *Dalton Trans.* **2016**, *45*, 6968–6973. [[CrossRef](#)] [[PubMed](#)]
45. Yang, Q.; Song, X.; Ge, J.; Zhao, G.; Zhang, W.; Xie, G.; Chen, S.; Gao, S. A 2D nickel-based energetic MOFs incorporating 3,5-diamino-1,2,4-triazole and malonic acid: Synthesis, crystal structure and thermochemical study. *J. Chem. Thermodyn.* **2016**, *92*, 132–138. [[CrossRef](#)]
46. Yue, Q.Y.; Lu, Y.M.; Chuan, F.X.; Yuan, D.; Chen, D.Y.; Yang, G.W.; Li, Q.Y. Synthesis, crystal structure, luminescence and thermal behavior of a new energetic zinc(II) compound. *Inorg. Chem. Commun.* **2016**, *68*, 68–71. [[CrossRef](#)]
47. Zhang, H.; Zhang, M.; Lin, P.; Malgras, V.; Tang, J.; Alshehri, S.M.; Yamauchi, Y.; Du, S.; Zhang, J. A highly energetic N-rich metal-organic framework as a new high-energy-density material. *Chem. Eur. J.* **2016**, *22*, 1141–1145. [[CrossRef](#)] [[PubMed](#)]
48. Zhang, J.; Du, Y.; Dong, K.; Su, H.; Zhang, S.; Li, S.; Pang, S. Taming dinitramide anions within an energetic metal-organic framework: A new strategy for synthesis and tunable properties of high energy materials. *Chem. Mater.* **2016**, *28*, 1472–1480. [[CrossRef](#)]
49. Zhang, Q.; Shreeve, J.M. Metal-organic frameworks as high explosives: A new concept for energetic materials. *Angew. Chem. Int. Ed.* **2014**, *53*, 2540–2542. [[CrossRef](#)] [[PubMed](#)]
50. Zhang, S.; Liu, X.; Liu, B.; Xia, Z.; Wang, W.; Yang, Q.; Ke, H.; Wei, Q.; Xie, G.; Chen, S. 3D Co(II, III) mixed-valence metal-organic framework affording field-induced slow magnetic relaxation. *Sci. China Chem.* **2015**, *58*, 1032–1038. [[CrossRef](#)]
51. Zhang, S.; Yang, Q.; Liu, X.; Qu, X.; Wei, Q.; Xie, G.; Chen, S.; Gao, S. High-energy metal-organic frameworks (HE-MOFs): Synthesis, structure and energetic performance. *Coord. Chem. Rev.* **2016**, *307*, 292–312. [[CrossRef](#)]
52. Wang, Y.; Zhang, J.; Su, H.; Li, S.; Zhang, S.; Pang, S. A simple method for the prediction of the detonation performances of metal-containing explosives. *J. Phys. Chem. A* **2014**, *118*, 4575–4581. [[CrossRef](#)] [[PubMed](#)]
53. Zhang, J.; Shreeve, J.M. 3D nitrogen-rich metal-organic frameworks: Opportunities for safer energetics. *Dalton Trans.* **2016**, *45*, 2363–2368. [[CrossRef](#)] [[PubMed](#)]
54. Deblitz, R.; Hrib, C.G.; Blaurock, S.; Jones, P.G.; Plenikowski, G.; Edlmann, F.T. Explosive werner-type cobalt(III) complexes. *Inorg. Chem. Front.* **2014**, *1*, 621–640. [[CrossRef](#)]
55. Evers, J.; Gospodinov, I.; Joas, M.; Klapotke, T.M.; Stierstorfer, J. Cocrystallization of photosensitive energetic copper(II) perchlorate complexes with the nitrogen-rich ligand 1,2-di(1H-tetrazol-5-yl)ethane. *Inorg. Chem.* **2014**, *53*, 11749–11756. [[CrossRef](#)] [[PubMed](#)]
56. Blair, L.H.; Colakel, A.; Vrcelj, R.M.; Sinclair, I.; Coles, S.J. Metal-organic fireworks: MOFs as integrated structural scaffolds for pyrotechnic materials. *Chem. Commun.* **2015**, *51*, 12185–12188. [[CrossRef](#)] [[PubMed](#)]
57. Friedrich, M.; Gálvez-Ruiz, J.C.; Klapötke, T.M.; Mayer, P.; Weber, B.; Weigand, J.J. BTA copper complexes. *Inorg. Chem.* **2005**, *44*, 8044–8052. [[CrossRef](#)] [[PubMed](#)]
58. Klapötke, T.M.; Mayer, P.; Stierstorfer, J.; Weigand, J.J. Bistetrazolylamines—Synthesis and characterization. *J. Mater. Chem.* **2008**, *18*, 5248. [[CrossRef](#)]
59. Guo, Y.; Gao, H.; Twamley, B.; Shreeve, J.M. Energetic nitrogen rich salts of *N,N*-bis[1(2)*H*-tetrazol-5-yl]amine. *Adv. Mater.* **2007**, *19*, 2884–2888. [[CrossRef](#)]
60. Guo, Y.; Tao, G.H.; Zeng, Z.; Gao, H.; Parrish, D.A.; Shreeve, J.M. Energetic salts based on monoanions of *N,N*-bis[1(2)*H*-tetrazol-5-yl]amine. *Chem. Eur. J.* **2010**, *16*, 3753–3762. [[CrossRef](#)] [[PubMed](#)]
61. Dong, L.L.; He, L.; Liu, H.Y.; Tao, G.H.; Nie, F.D.; Huang, M.; Hu, C.W. Nitrogen-rich energetic ionic liquids based on the *N,N*-bis[1*H*-tetrazol-5-yl]amine anion—Syntheses, structures, and properties. *Eur. J. Inorg. Chem.* **2013**, 5009–5019. [[CrossRef](#)]
62. Xue, B.D.; Yang, Q.; Chen, S.P.; Gao, S.L. Synthesis, crystal structure, and thermodynamics of a high-nitrogen copper complex with *N,N*-bis[1(2)*H*-tetrazol-5-yl] amine. *J. Therm. Anal. Calorim.* **2010**, *101*, 997–1002. [[CrossRef](#)]
63. Li, N.; Chen, W.B.; Guan, Y.F.; OuYang, Z.J.; Dong, W. Chlorine anion- π and $\pi^- - \pi^-$ interactions in two tetrazolyl derivative based Cu^{2+} complexes and quantum chemical calculations. *Inorg. Chim. Acta* **2014**, *409*, 349–352. [[CrossRef](#)]
64. Qu, B.; Lu, X.; Wu, Y.; You, X.; Xu, X. Synthesis of copper micro-rods with layered nano-structure by thermal decomposition of the coordination complex $\text{Cu}(\text{BTA})_2$. *Nanoscale Res. Lett.* **2015**, *10*, 1–5. [[CrossRef](#)] [[PubMed](#)]
65. Cook, C.; Habib, F.; Aharen, T.; Clerac, R.; Hu, A.; Murugesu, M. High-temperature spin crossover behavior in a nitrogen-rich Fe(III)-based system. *Inorg. Chem.* **2013**, *52*, 1825–1831. [[CrossRef](#)] [[PubMed](#)]

66. Liu, N.; Yue, Q.; Wang, Y.Q.; Cheng, A.L.; Gao, E.Q. Coordination compounds of bis(5-tetrazolyl)amine with manganese(II), zinc(II) and cadmium(II): Synthesis, structure and magnetic properties. *Dalton Trans.* **2008**, *34*, 4621–4629. [CrossRef] [PubMed]
67. Lu, Y.B.; Wang, M.S.; Zhou, W.W.; Xu, G.; Guo, G.C.; Huang, J.S. Novel 3-D PtS-like tetrazolate-bridged manganese(II) complex exhibiting spin-canted antiferromagnetism and field-induced spin-flop transition. *Inorg. Chem.* **2008**, *47*, 8935–8942. [CrossRef] [PubMed]
68. Jiang, T.; Zhang, X.M. Temperature tuned synthesis of zinc *N,N*-bis[1(2)*H*-tetrazol-5-yl]-amine complexes: From Zn₃O cluster-based 3-connected 63-hcb and (3,6)-connected (43)2(46)-kgd layers to Zn₅(OH)₄ chain-based 3D open framework. *Cryst. Growth Des.* **2008**, *8*, 3077–3083. [CrossRef]
69. Li, F.; Bi, Y.; Zhao, W.; Zhang, T.; Zhou, Z.; Yang, L. Nitrogen-rich salts based on the energetic [monoquabis *N,N*-bis[1(2)*H*-tetrazol-5-yl] amine]-zinc(II)] anion: A promising design in the development of new energetic materials. *Inorg. Chem.* **2015**, *54*, 2050–2057. [CrossRef] [PubMed]
70. Lin, J.M.; Guan, Y.F.; Wang, D.Y.; Dong, W.; Wang, X.T.; Gao, S. Syntheses, structures and properties of seven isomorphous 1D Ln³⁺ complexes Ln(BTA)(HCOO)(H₂O)₃ (H₂BTA = bis(tetrazolyl)amine, Ln = Pr, Gd, Eu, Tb, Dy, Er, Yb) and two 3D Ln³⁺ complexes Ln(HCOO)₃ (Ln = Pr, Nd). *Dalton Trans.* **2008**, *44*, 6165–6169. [CrossRef] [PubMed]
71. Wang, W.; Chen, S.; Gao, S. Syntheses and characterization of lead(II) *N,N*-bis[1(2)*H*-tetrazol-5-yl] amine compounds and effects on thermal decomposition of ammonium perchlorate. *Eur. J. Inorg. Chem.* **2009**, *2009*, 3475–3480. [CrossRef]
72. Wu, J.T.; Zhang, J.G.; Yin, X.; He, P.; Zhang, T.L. Synthesis and characterization of the nitrophenol energetic ionic salts of 5,6,7,8-tetrahydrotetrazolo[1,5-*b*][1,2,4]triazine. *Eur. J. Inorg. Chem.* **2014**, *2014*, 4690–4695. [CrossRef]
73. Liu, Q.; Jin, B.; Peng, R.; Guo, Z.; Zhao, J.; Zhang, Q.; Shang, Y. Synthesis, characterization and properties of nitrogen-rich compounds based on cyanuric acid: A promising design in the development of new energetic materials. *J. Mater. Chem. A* **2016**, *4*, 4971–4981. [CrossRef]
74. Allen, F.H.; Kennard, O.; Watson, D.G.; Brammer, L.; Orpen, A.G.; Taylor, R. Tables of bond lengths determined by X-ray and neutron diffraction. Part I. Bond lengths in organic compounds. *J. Chem. Soc. Perkin Trans. 2* **1987**, S1–S19. [CrossRef]
75. Li, F.; Zhao, W.; Chen, S.; Zhang, T.; Zhou, Z.; Yang, L. Nitrogen-rich alkali metal salts (Na and K) of [bis(*N,N*-bis[1*H*-tetrazol-5-yl] amine)-zinc(II)] anion: Syntheses, crystal structures, and energetic properties. *Z. Anorg. Allg. Chem.* **2015**, *641*, 911–916. [CrossRef]
76. Cacho-Bailo, F.; Téllez, C.; Coronas, J. Interactive Thermal Effects on Metal-Organic Framework Polymer Composite Membranes. *Chem. Eur. J.* **2016**, *22*, 9533–9536. [CrossRef] [PubMed]
77. Kissinger, H.E. Reaction kinetics in differential thermal analysis. *Anal. Chem.* **1957**, *29*, 1702–1706. [CrossRef]
78. Doyle, C.D. Kinetic analysis of thermogravimetric data. *J. Appl. Polym. Sci.* **1961**, *5*, 285–292. [CrossRef]
79. Ozawa, T. A new method of analyzing thermogravimetric data. *Bull. Chem. Soc. Jpn.* **1965**, *38*, 1881–1886. [CrossRef]
80. Geetha, M.; Nair, U.R.; Sarwade, D.B.; Gore, G.M.; Asthana, S.N.; Singh, H.J. Studies on CL-20: The most powerful high energy material. *J. Therm. Anal. Calorim.* **2003**, *73*, 913–922. [CrossRef]
81. Turcotte, R.; Vachon, M.; Kwok, Q.S.; Wang, R.; Jones, D.E. Thermal study of HNIW (CL-20). *Thermochim. Acta* **2005**, *433*, 105–115. [CrossRef]
82. Sheldrick, G.M. *SHELXS-97, Program for Crystal Structure Solution*; University of Göttingen: Göttingen, Germany, 1997.
83. Sheldrick, G.M. *SHELXS-97, Program for Crystal Structure Refinement*; University of Göttingen: Göttingen, Germany, 1997.
84. Delley, B. An all-electron numerical method for solving the local density functional for polyatomic molecules. *J. Chem. Phys.* **1990**, *92*, 508–517. [CrossRef]
85. Monkhorst, H.J.; Pack, J.D. Special points for Brillouin-zone integrations. *Phys. Rev. B* **1976**, *13*, 5188–5192. [CrossRef]
86. Perdew, J.P.; Burke, K.; Ernzerhof, M. Generalized gradient approximation made simple. *Phys. Rev. Lett.* **1996**, *77*, 3865–3868. [CrossRef] [PubMed]

